

Pseudopotential density functional treatment of atoms and molecules in cartesian coordinate grid

Amlan K. Roy*

Department of Chemistry, University of Kansas, Lawrence, KS, 66045, USA.[†]

Abstract

This is a follow-up of our recently proposed work on pseudopotential calculation (Ref. [21]) of atoms and molecules within DFT framework, using cartesian coordinate grid. Detailed results are presented to demonstrate the usefulness, applicability of the same for a larger set of species (5 atoms; 53 molecules) and exchange-correlation functionals (local, nonlocal). A thorough comparison on total, component, ionization, atomization energies, eigenvalues, potential energy curves with available literature data shows excellent agreement. Additionally, HOMO energies for a series of molecules show significant improvements by using the Leeuwen-Baerends exchange potential, compared to other functionals considered. Comparison with experiments has been made, wherever possible.

*Present address: Indian Institute of Science Education and Research (IISER), Division of Chemical Sciences, Block HC, Sector III, Salt Lake City, Kolkata-700106.

[†]Electronic address: akroy@chem.ucla.edu, akroy@iiserkol.ac.in

I. INTRODUCTION

Development of accurate efficient methods for the electronic structure of molecules, solids, clusters has been a topic of increasingly intense interest in chemistry, physics, materials science, etc. In the past two decades, density functional theory (DFT) has been applied with remarkable success to investigate the structural (such as geometries, vibrational frequencies, energetics of chemical reactions, etc.) as well as dynamical (such as photoabsorption, photoemission, multi-photon ionization, high-order harmonic generation, etc.) characteristics of such systems. In essence, the ground-state electronic energy is partitioned as: $E[\rho(\mathbf{r})] = T_s[\rho(\mathbf{r})] + U[\rho(\mathbf{r})] + E_{xc}[\rho(\mathbf{r})]$, where the three terms in the right-hand side denote kinetic energy of a system of non-interacting particles of same density $\rho(\mathbf{r})$, classical electrostatic energy (including electron-nuclear attraction, electron-electron and nuclear-nuclear repulsion), and exchange-correlation (XC) energy respectively. The single-particle wave functions are obtained from the Kohn-Sham (KS) equation as:

$$\left[\frac{1}{2} \nabla^2 + v_{eff}(\mathbf{r}) \right] \psi_i(\mathbf{r}) = \epsilon_i \psi_i(\mathbf{r}) \quad (1)$$

where $v_{eff}(\mathbf{r})$ contains the relevant one- and two-body potentials, while the electron density is given by the squared sum of the occupied orbitals, $\rho(\mathbf{r}) = \sum_i f_i |\psi_i(\mathbf{r})|^2$.

Broadly speaking, two approaches have gained popularity for the practical solution of above KS equation. In the *real-space method* [1–5] the discretized KS equation is solved iteratively on a mesh using either finite-difference, finite-element or wavelets. The grid-based matrix presentation produces *structured, highly banded* matrices. Moreover, the near *locality* (the potential operator is diagonal in coordinate space whereas the Laplacian operator is nearly local) can potentially remove the omnipresent nagging problem arising due to the basis-set incompleteness in the contrasting basis-set approaches. Furthermore, they are easily amenable to the so-called linear-scaling methods. While such schemes usually require a larger number of grids to achieve physically meaningful results, through introduction of higher-order and multigrid techniques, the effective grid can be reduced significantly. In *basis-set* approaches, on the other hand, the single-particle wave functions are represented by a variety of functions such as Slater-type orbitals, gaussian type functions (GTF), numerical functions, plane waves (PW), augmented plane waves, linear muffin-tin orbitals etc. While currently, there is a preponderance of the atom-centered localized GTFs in the field of molecular quantum chemistry [6] (chiefly due their ability to deal with some of the important

multi-center integrals analytically), *ab initio* calculation in the condensed matter regime is almost exclusively dominated by the PWs [7] (mainly because the Fast-Fourier transform (FFT) technique can be employed to take advantage of the periodicity of such systems). This work is concerned with the basis-set approach to tackle the electron-structure calculation of atoms and molecules. Recently there has been effort to combine the basis sets; e.g., in [8], a gaussian basis set was used to expand the KS molecular orbital (MO), whereas an *auxiliary* augmented PW basis was utilized to express the electronic charge density.

Excepting a very few attempts such as the *grid-free* approach [9], that uses a resolution of identity to evaluate multi-center integrals over functionals at the expense of an *auxiliary* basis set, a large majority of basis-set-based molecular DFT calculations employ some carefully selected suitable 3D quadrature for a sensible choice of grid points in space. A very successful common scheme [10] involves partitioning the 3D molecular integrand into single-center discrete atomic “cells”. These can be treated using standard numerical techniques individually and then summing these up using some appropriate weight functions leads to the desired final result. In this so-called atom-centered grid (ACG) method, the mono-centric atomic integrals are computed by separating the radial and angular components. The former has typically been performed by introducing several quadratures and various mapping schemes. Some of these are Gauss-Chebyshev quadrature of second kind, Chebyshev quadratures of first and second kind, Gaussian quadrature, Euler-MacLaurin formula, numerical quadratures, etc. [11–15]. Angular integrations are handled usually by the Lebedev spherical method [16–18]. In another development, [19] 3D integration of molecular integrands were performed numerically based on a division of space and subsequent integration over the resulting regions by product Gauss rule. A variational integration mesh [20], which depends on the position of individual atoms has also been reported by breaking the space into three different regions, *viz.*, atomic spheres, excluded cubic region and interstitial parallelepiped. Other numerical grids [21] have been proposed as well for gaussian basis set calculations. Recently there has been an attempt to connect the cartesian coordinate grid (CCG) and ACG by a divided-difference polynomial interpolation which can translate the electron density and gradients from the former to the latter [22].

In a previous article [23], henceforth referred to as I, efforts were made to employ the CCGs in the context of atoms and molecules within the linear combination of GTF ansatz of DFT. In this work, respective quantities such as the localized atom-centered basis set, the

two-body classical Coulomb repulsion and the non-classical XC potentials were directly set up on the 3D CCG. Local-density approximated (LDA) XC functionals of the homogeneous electron gas in conjunction with the Hay-Wadt type pseudopotential was used. A multitude of quantities like *viz.*, individual energy contributions to total energy, eigenvalues, potential energy curves, ionization energies, as well as atomization energies were investigated. The relevance and performance of the CCGs were judged on 12 molecules (from small to medium size) and 3 atoms. In each of these cases practically identical results as those from the ACG and grid-free results were obtained. Now, it is well-known that the local density functionals suffer from a number of problems and hence it is essential to use more accurate functionals, namely those incorporating the gradient and Laplacian corrections. We have a number of objectives in this article. Firstly, we want to assess the validity and efficacy of the aforementioned scheme of I for a larger set of species to justify and validate its future usage. Secondly its scope of applicability is broadened by incorporating the gradient corrected XC functionals (for demonstration, the popular non-local Becke exchange [24] and Lee-Yang-Parr (LYP) correlation [25] is used). First, a detailed test on the convergence of our results on 5 atoms and 12 molecules is made as in I for the BLYP XC functional. In the next step, additional 41 molecules are considered both at the LDA and BLYP level. Detailed comparison with reference theoretical and experimental results are made, wherever possible. Besides, we also report the highest-occupied molecular orbital (HOMO) energies obtained with the Leeuwen-Baerends (LB) [26, 27] exchange potential for the latter 41 molecules (see Section III for motivational details). In all cases, this significantly improves both LDA and BLYP HOMO energies. Section II gives a summary of the method of calculation and computational aspects. Section III presents a discussion on the results obtained. We end with a few concluding remarks about the future prospects in Section IV.

II. METHODOLOGY AND IMPLEMENTATION

This section sketches the essential steps involved in the ground-state calculation of a many-electron system within the KS DFT framework used in the present work; further details can be found in [23].

The KS MOs $\{\psi_i^\sigma(\mathbf{r})\}$, $\sigma = \alpha, \beta$ are linearly expanded in terms of a set of K known basis

functions as,

$$\psi_i^\sigma(\mathbf{r}) = \sum_{\mu=1}^K C_{\mu i}^\sigma \chi_\mu(\mathbf{r}), \quad i = 1, 2, \dots, K \quad (2)$$

where the set $\{\chi_\mu(\mathbf{r})\}$ denotes the contracted gaussian functions centered on the constituent atoms while $\{C_{\mu i}^\sigma\}$ contains the contraction coefficients for the orbital $\psi_i^\sigma(\mathbf{r})$. The individual spin-densities are given by,

$$\rho^\sigma(\mathbf{r}) = \sum_i^{N^\sigma} |\psi_i^\sigma(\mathbf{r})|^2 = \sum_\mu \sum_\nu P_{\mu\nu}^\sigma \chi_\mu(\mathbf{r}) \chi_\nu^*(\mathbf{r}) \quad (3)$$

where P^σ stands for the respective density matrices.

Substitution of these terms into the energy expression, followed by minimization with respect to unknown coefficients $C_{\mu i}^\sigma$, subject to the orthogonality constraint leads to the following matrix KS equation which is akin to the unrestricted Pople-Nesbet equation in Hartree-Fock (HF) theory,

$$\mathbf{F}^\sigma \mathbf{C}^\sigma = \mathbf{S} \mathbf{C}^\sigma \epsilon^\sigma. \quad (4)$$

Here \mathbf{S} and \mathbf{F} denote the $K \times K$ real, square symmetric overlap and total KS matrices respectively. \mathbf{C} stands for the eigenvector matrix containing the expansion coefficients $C_{\mu i}^\sigma$ while the orbital energies ϵ_i are embedded in the diagonal matrix ϵ . The KS matrix is conveniently written as,

$$F_{\mu\nu}^\sigma = H_{\mu\nu}^{\text{core}} + J_{\mu\nu} + F_{\mu\nu}^{XC\sigma} \quad (5)$$

where the first two terms in the right-hand side signify the matrices of one-electron bare-nucleus Hamiltonian and the classical Coulomb repulsion. The one-electron overlap, kinetic-energy and nuclear-attraction integrals involved are the same as encountered in the GTF-based HF schemes and are computed using standard recursion algorithm [28, 29]. The pseudopotential matrix elements in the gaussian basis are taken from the GAMESS quantum chemistry program output [30]. The Coulomb potential is evaluated using a Fourier convolution technique [31, 32], which effectively uses a Ewald summation type decomposition in terms of short- and long-range contributions,

$$\frac{1}{r} = \frac{\text{erf}(\alpha r)}{r} + \frac{\text{erfc}(\alpha r)}{r} = v_c^{\text{long}}(r) + v_c^{\text{short}}(r). \quad (6)$$

Here erf(x) and erfc(x) identify the error function and complimentary error function respectively. Note that the latter goes to zero exponentially fast at large r . The parameter α controls the range on which v_c^{short} is nonzero. After a thorough check on the convergence

with respect to α , a value within the range of 6–8 seemed satisfactory and we employed 7 for all the results reported in this work. This has produced highly satisfying results for a modest number of atomic (3) and molecular (12) systems in our previous work [23]. The short-range Fourier integral is calculated analytically, whereas the long-range part is obtained from FFT of the real-space values.

As already mentioned, a major thrust of the current communication is to demonstrate the feasibility and viability of our current scheme in the context of so-called “non-local” (gradient and Laplacian-dependent) XC functionals which would be necessary for future chemical applications. For this, we first test this with two of the widely used functionals, namely the Becke exchange [24] and LYP correlation [25] (for convenience, an alternative equivalent form [33] containing only the first derivative has been mostly used in practice). The homogeneous electron-gas correlation of Vosko-Wilk-Nusair (VWN) [34] is used in all the LDA calculations. Following [35], the gradient-dependent functionals can be treated without evaluating the density Hessians by using a finite-orbital basis expansion. To this end, XC contributions of the KS matrix is written in the following working form,

$$F_{\mu\nu}^{XC\alpha} = \int \left[\frac{\partial f}{\partial \rho_\alpha} \chi_\mu \chi_\nu + \left(2 \frac{\partial f}{\partial \gamma_{\alpha\alpha}} \nabla \rho_\alpha + \frac{\partial f}{\partial \gamma_{\alpha\beta}} \nabla \rho_\beta \right) \cdot \nabla (\chi_\mu \chi_\nu) \right] d\mathbf{r} \quad (7)$$

where $\gamma_{\alpha\alpha} = |\nabla \rho_\alpha|^2$, $\gamma_{\alpha\beta} = \nabla \rho_\alpha \cdot \nabla \rho_\beta$, $\gamma_{\beta\beta} = |\nabla \rho_\beta|^2$ and f is a function only of the local quantities ρ_α , ρ_β and their gradients. The BLYP functionals are implemented using the Density Functional Repository program [36]. The two-electron matrix elements cannot be evaluated analytically; here we use direct numerical integrations on the CCG grid. Note that some of the existing DFT codes [37] use an alternative route of fitting these by an auxiliary basis set, the so-called discrete variational method [38–40]. The generalized matrix-eigenvalue problem is solved using the standard LAPACK routine [41] accurately efficiently. Self-consistent set of MOs, density and energy are obtained in the usual manner subject to the convergence of (a) potential (b) total energy and (c) eigenvalues. Tolerance of 10^{-6} a.u. was used for (b) and (c), while a value of 10^{-5} for (a). Atomic units employed, unless otherwise mentioned.

III. RESULTS AND DISCUSSION

At first, Table I shows a comparison of our calculated ground-state energy components with respect to the number of mesh points $N_r (r \in \{x, y, z\})$ as well as the grid spacing h_r , for Cl_2 and HCl at internuclear distances 4.2 and 2.4 a.u. respectively employing the BLYP density functional. In this occasion, we adopt a similar presentation strategy as in I. A series of calculations were performed in the same fashion to test the convergence of our results with respect to the grid parameters. These numerical experiments produced very similar conclusions as reached in for LDA XC-case in I. Hence out of eight, we eventually report here the results from two such sets only (to avoid too many entries in the table), *viz.*, (i) Set A with $N_r = 64$, $h_r = 0.3$, (ii) Set B with $N_r = 128$, $h_r = 0.2$, which suffices to illustrate the important points. The reference theoretical results presented in this and all other tables throughout the article imply those obtained from the GAMESS quantum chemistry program [30]. They use same basis set, effective core potential and employing the “grid” option. The corresponding results from the “gridfree” option are quoted in footnotes for convenience, in several occasions. Now onwards, we will refer to them as *grid* and *grid-free* theoretical reference results. The former uses the Euler-McLaurin quadrature for the radial integrations and Gauss-Legendre quadrature for the angular integrations. The convergence of energies and other quantities with respect to the radial and angular grid was monitored by performing two extra set of calculations (i) $N_r, N_\theta, N_\phi = 96, 36, 72$ (ii) $N_r, N_\theta, N_\phi = 128, 36, 72$, besides the default grid option ($N_r, N_\theta, N_\phi = 96, 12, 24$), where the three integers denote the respective number of integration points in r, θ, ϕ directions. Note that all the 3 grids offered very similar results; for example, out of the 17 atoms and molecules, total energies remain same upto 5th decimal place for 8 species for all 3 grids. In the remaining cases, they differed slightly among each other as the grid parameters changed; the largest deviation in total energy being 0.00064 a.u. for Na_2Cl_2 and for all others it is well below 0.00007 a.u. However, passing from the default grid to (ii) gradually improves N . In this and all other tables in the article, we have quoted (ii) results for the reference *grid*-DFT values. The *grid-free* implementation uses the resolution of identity to simplify the molecular integrals enabling their analytical evaluation and obviating the necessity of using grid quadratures. Quantities considered are the same as those in I, *viz.*, various energies such as kinetic (T), total nucleus-electron attraction (V_t^{ne}), classical Coulomb repulsion (E_h), exchange (E_x),

TABLE I: Variation of the energy components and N with respect to the grid parameters for Cl_2 and HCl with reference values. BLYP results in a.u.

Set	Cl_2 ($R = 4.2$ a.u.)			HCl ($R = 2.4$ a.u.)		
	A	B	Ref. [30]	A	B	Ref. [30]
N_r	64	128		64	128	
h_r	0.3	0.2		0.3	0.2	
$\langle T \rangle$	11.21504	11.21577	11.21570	6.25431	6.25464	6.25458
$\langle V_t^{ne} \rangle$	-83.72582	-83.72695	-83.72685	-37.29933	-37.29987	-37.29979
$\langle E_h \rangle$	36.74464	36.74501		15.86078	15.86103	
$\langle E_x \rangle$	-5.29009	-5.29015		-3.01023	-3.01026	
$\langle E_c \rangle$	-0.37884	-0.37892		-0.21171	-0.21174	
$\langle V_t^{ee} \rangle$	31.07572	31.07594	31.07594	12.63884	12.63903	12.63901
$\langle E_{nu} \rangle$	11.66667	11.66667	11.66667	2.91667	2.91667	2.91667
$\langle V \rangle$	-40.98344	-40.98434	-40.98424	-21.74382	-21.74417	-21.74411
$\langle E_{el} \rangle$	-41.43506	-41.43524	-41.43522	-18.40618	-18.40620	-18.40620
$\langle E \rangle$	-29.76840	-29.76857	-29.76855 ^a	-15.48951	-15.48953	-15.48953 ^b
N	14.00006	14.00000	13.99998	8.00002	8.00000	8.00000

^aThe *grid-free* DFT value is -29.74755 a.u. [30].

^bThe *grid-free* DFT value is -15.48083 a.u. [30].

correlation (E_c), total two-electron potential (V_t^{ee}), nuclear repulsion (E_{nu}), total potential (V), electronic (E_{el}) and total energy (E) respectively, as well as the integrated electron density N . Evidently, as in the LDA case, both sets offer excellent agreement in total energies and component energies with literature values for both molecules. The individual two-body energy terms were not available in the reference output and thus could not be directly compared. As expected, for obvious reasons Set B results are closer to reference values than Set A, but only marginally. For Cl_2 this is slightly more pronounced than that for HCl . Absolute deviations in total energy for Set B for Cl_2 and HCl are only 0.00002 and 0.00000 a.u. respectively. In both cases, there is slight improvement in N , as we move from Set A to B. For all practical purposes, Set A is adequate enough for both of them. Note that reference *grid-free* DFT energies differ substantially from the corresponding *grid*-DFT values.

To further demonstrate the accuracy and reliability of present results, in Table II, calculated negative eigenvalues for Cl_2 and HCl (using BLYP XC combination) are presented at the same geometries of previous table, along with those obtained from reference [30]. Once again, excellent agreement is observed for both molecules. Sets A and B results match

TABLE II: Comparison of the calculated negative eigenvalues of Cl₂ and HCl with the reference values. BLYP results are given in a.u.

MO	Cl ₂ ($R = 4.2$ a.u.)			MO	HCl ($R = 2.4$ a.u.)		
	A	B	Ref. [30]		A	B	Ref. [30]
Set							
$2\sigma_g$	0.8143	0.8143	0.8143	2σ	0.7707	0.7707	0.7707
$2\sigma_u$	0.7094	0.7094	0.7094	3σ	0.4168	0.4167	0.4167
$3\sigma_g$	0.4170	0.4171	0.4171	$1\pi_x$	0.2786	0.2786	0.2786
$1\pi_{xu}$	0.3405	0.3405	0.3405	$1\pi_y$	0.2786	0.2786	0.2786
$1\pi_{yu}$	0.3405	0.3405	0.3405				
$1\pi_{xg}$	0.2778	0.2778	0.2778				
$1\pi_{yg}$	0.2778	0.2778	0.2778				

completely with literature values for *all* the orbital energies except the lone case of $3\sigma_g$ for Cl₂ (Set A), where the absolute deviation is only 0.0001 a.u.

Now Table III tabulates our computed negative total energies of Cl₂ (relative to -29 a.u. in columns 2–3, left panel) and HCl (relative to -15 a.u. in columns 6–7, right panel) for Sets A and B using the BLYP XC functionals. A broad range of internuclear distance is considered in columns 1 and 5 (3.5–5.0 a.u. for the former and 1.5–3.0 a.u. for the latter) and the corresponding *grid* DFT results obtained from the GAMESS program [30] are listed in columns 5 and 8 for comparison. These are depicted vividly for smaller ranges of R in Fig. 1. Clearly, for both the molecules, Sets A and B results are practically coincident on reference values for the entire range of R . For Cl₂, maximum absolute deviation is 0.0001 a.u. with Set B and 0.0002 a.u. (only in 2 instances) with Set A. However, for HCl, the two corresponding maximum deviations are 0.0001 a.u., for both sets. This is anticipated from the results of Table I, where we noticed results from these two sets confirmed to each other more for HCl than for Cl₂. This discussion clearly illustrates the faithfulness of current calculation.

For additional test, Table IV reports kinetic, potential and total energies as well as N for 15 species (5 atoms and 10 molecules) calculated using the BLYP XC functional. With the exception of Mg and S, these are the same species studied in Table V of I, using the LDA XC functionals. In this and all other tables henceforth, the experimental geometries in the NIST database [42] are used. The component energies show similar agreements with the reference values; hence omitted to avoid crowding. The respective *grid*-DFT results obtained from [30] are presented side by side for comparison. These are ordered in terms of

TABLE III: Calculated potential energy curves of Cl₂ and HCl for grid Sets A, B, along with literature values (grid-DFT). Negative values are given in a.u.

R (a.u.)	Cl ₂ (Total energy relative to -29 a.u.)			R (a.u.)	HCl (Total energy relative to -15 a.u.)		
	A	B	Ref. [30]		A	B	Ref. [30]
3.50	0.7032	0.7032	0.7033	1.50	0.0533	0.0534	0.0533
3.60	0.7231	0.7232	0.7231	1.60	0.1818	0.1818	0.1818
3.70	0.7383	0.7384	0.7384	1.70	0.2767	0.2767	0.2767
3.80	0.7497	0.7498	0.7497	1.80	0.3464	0.3464	0.3464
3.90	0.7579	0.7580	0.7579	1.90	0.3969	0.3969	0.3969
4.00	0.7635	0.7635	0.7635	2.00	0.4328	0.4328	0.4329
4.10	0.7668	0.7669	0.7669	2.10	0.4578	0.4577	0.4577
4.20	0.7684	0.7686	0.7685	2.20	0.4741	0.4742	0.4742
4.30	0.7686	0.7688	0.7687	2.30	0.4842	0.4842	0.4842
4.40	0.7676	0.7678	0.7678	2.40	0.4895	0.4895	0.4895
4.50	0.7658	0.7659	0.7659	2.50	0.4912	0.4912	0.4912
4.60	0.7632	0.7633	0.7633	2.60	0.4903	0.4903	0.4903
4.70	0.7599	0.7601	0.7601	2.70	0.4874	0.4874	0.4874
4.80	0.7565	0.7566	0.7566	2.80	0.4831	0.4831	0.4831
4.90	0.7527	0.7528	0.7528	2.90	0.4778	0.4778	0.4778
5.00	0.7486	0.7487	0.7488	3.00	0.4718	0.4718	0.4718

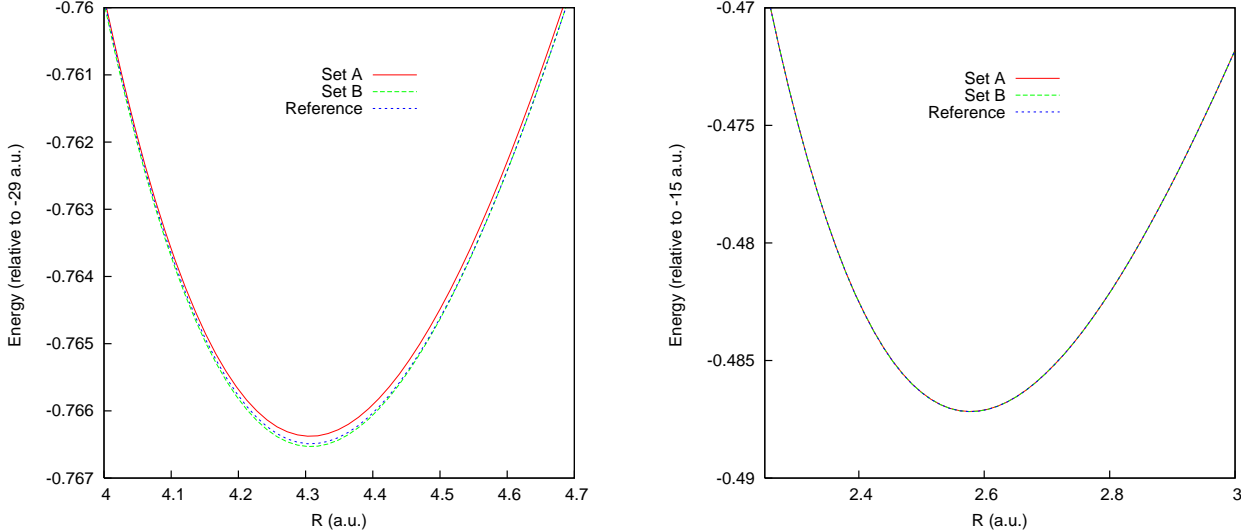


FIG. 1: Potential energy curves for Cl₂ (left panel) and HCl (right panel) for grid Sets A, B. Reference grid-DFT results are also given for comparison.

increasing N as descending the table. First 10 of these use the same grid parameters as in Table V of I, i.e., $N_r = 64, h_r = 0.4$, whereas for last 5 we use $N_r = 128, h_r = 0.3$. Overall, the agreement of our results with the reference is excellent. In several occasions (such as Na₂, P, As, Na₂Cl₂), the total energies completely match with them. The largest absolute

TABLE IV: Comparison of the kinetic ($\langle T \rangle$), potential ($\langle V \rangle$), total (E) energies and N for several atoms and molecules with the reference grid-DFT results [30]. BLYP results in a.u. PW=Present Work. See text for details.

System	$\langle T \rangle$		$-\langle V \rangle$		$-\langle E \rangle$		N	
	PW	Ref. [30]	PW	Ref. [30]	PW	Ref. [30]	PW	Ref. [30]
Na ₂	0.14723	0.14723	0.52871	0.52871	0.38148	0.38148	1.99999	2.00000
Mg	0.24935	0.24935	1.06017	1.06017	0.81082	0.81083	1.99999	1.99999
NaH	0.60093	0.60088	1.34698	1.34693	0.74606	0.74605	1.99997	1.99999
P	2.38891	2.38890	8.78249	8.78248	6.39358	6.39358	4.99999	4.99999
As	2.10490	2.10494	8.14207	8.14211	6.03717	6.03717	4.99999	4.99999
S	3.73143	3.73145	13.73598	13.73599	10.00455	10.00454	6.00000	5.99999
Br	4.27022	4.27043	17.36122	17.36148	13.09100	13.09105	7.00000	6.99999
NaCl	5.83959	5.83957	21.01698	21.01694	15.17739	15.17737	8.00003	7.99999
H ₂ S	4.98071	4.98066	16.21919	16.21913	11.23848	11.23846	8.00000	7.99999
PH ₃	4.18229	4.18224	12.40101	12.40096	8.21871	8.21872	7.99999	7.99999
Br ₂	8.66533	8.66527	34.88603	34.88596	26.22070	26.22069	13.99999	14.00000
H ₂ S ₂	8.88238	8.88240	30.16535	30.16538	21.28297	21.28298	13.99999	13.99999
MgCl ₂	11.75947	11.75999	42.54049	42.54103	30.78102	30.78104	16.00004	15.99999
Na ₂ Cl ₂	11.68815	11.68842	42.12410	42.12438	30.43595	30.43595	16.00002	15.99999
SiH ₂ Cl ₂	14.14948	14.14945	49.04463	49.04461	34.89515	34.89516	19.99999	20.00000

deviation in total energy is only 0.0013% (for NaH).

Table V displays the calculated negative HOMO energies, $-\epsilon_{\text{HOMO}}$ (in a.u.) and estimated atomization energies (in kcal/mole) for the same 12 molecules in Table V of I, using the BLYP XC density functional. These are compared with the theoretical [30] as well the experimental results from the NIST database [43]. Same grid parameters as those in the previous table are employed for these. The $-\epsilon_{\text{HOMO}}$ values completely agree with those from the theoretical literature results [30], except in two occasions (MgCl₂, Na₂Cl₂), where the absolute discrepancy remains only 0.0001 a.u. The calculated atomization energies also show very good agreement with the reference theoretical values [30]. For Na₂ HCl, NaCl and H₂S, our values are identical as those from reference. The largest discrepancy (0.248%) is observed for Br₂. However, both quantities differ significantly from the experimental values; but that is a separate issue (not directly related to the main theme of this work). These could possibly be improved further by employing more appropriate basis functions and/or better XC functionals, and may be considered in future works.

The previous work of [23] as well as the ongoing discussion amply demonstrates that the approach can produce good-quality results for both LDA and gradient-corrected non-local

TABLE V: Comparison of $-\epsilon_{\text{HOMO}}$ (a.u.) and atomization energies (kcal/mole) for molecules with the literature data using BLYP XC functional. PW=Present Work. 1 a.u.= 627.509471 kcal/mole.

See text for details.

System	$-\epsilon_{\text{HOMO}}$ (a.u.)			Atomization energy(kcal/mol)		
	PW	Theory [30]	Expt. [43]	PW	Theory [30]	Expt. [43]
Na ₂	0.1002	0.1002	0.1798	11.51	11.51	17.0
NaH	0.1421	0.1421	—	45.37	45.36	47.2
HCl	0.2785	0.2785	0.4683	89.88	89.88	102.2
NaCl	0.1733	0.1733	0.3381	88.75	88.75	97.4
H ₂ S	0.2190	0.2190	0.3843	156.59	156.59	173.2
PH ₃	0.2287	0.2287	0.3627	218.72	218.73	227.1
Cl ₂	0.2652	0.2652	0.4219	22.89	22.90	57.2
Br ₂	0.2451	0.2451	0.3865	24.28	24.22	45.4
H ₂ S ₂	0.2288	0.2288	0.3418	181.66	181.68	229.6
MgCl ₂	0.2697	0.2698	—	164.04	164.07	187.4
Na ₂ Cl ₂	0.2020	0.2021	—	228.43	228.46	243.1
SiH ₂ Cl ₂	0.2836	0.2836	0.4300	287.92	287.95	341.8

XC functionals for atoms and small-to-medium molecules, within the specifics of basis set. This is further validated in Table VI where both LDA and BLYP results are reported for 41 extra molecules to illustrate the broad scope its applicability. The experimental geometries are again taken from the NIST database [42]. The kinetic, potential, total energy and N are presented. Since it has been clearly established that our obtained results are sufficiently accurate, here we omit the reference theoretical values. Only some random checks were made to ensure that this is indeed the case. First 29 molecules from top were treated using $N_r = 64, h_r = 0.4$, while for the remaining 12, we used $N_r = 128, h_r = 0.3$ grid. On the light of all the results and discussion so far, we believe that these represent the correct values.

Finally Table VII compares the calculated $-\epsilon_{\text{HOMO}}$ (in a.u.) and atomization energies (in kcal/mole) with the literature data, for the same molecules at same geometries as in previous table. Experimental results, wherever available, are quoted from [43]. In this case also, reference results are omitted to avoid crowding. But as expected, they show very little deviation from ours. An asterisk in the experimental atomization energies denote the values at 298°K; otherwise they imply 0°K values. Both LDA and BLYP results are given for these quantities side by side. However for the former we also include results obtained with another exchange functional for the following reason. It is well-known that the XC potentials derived from the simplest LDA or generalized gradient approximation (GGA) suffer

TABLE VI: Kinetic ($\langle T \rangle$), potential ($\langle V \rangle$), total (E) energies and N for several molecules. LDA and BLYP results are given in a.u. PW=Present Work. See text for details.

System	$\langle T \rangle$		$-\langle V \rangle$		$-\langle E \rangle$		N	
	LDA	BLYP	LDA	BLYP	LDA	BLYP	LDA	BLYP
Mg ₂	0.50225	0.50973	2.12547	2.13172	1.62322	1.62199	3.99999	3.99999
MgH ₂	1.32435	1.38562	3.25978	3.35466	1.93543	1.96904	3.99999	3.99999
AlH	1.21615	1.25090	3.71761	3.77090	2.50147	2.52000	3.99999	3.99999
SiH	1.92640	1.96967	6.25051	6.31591	4.32411	4.34625	4.99999	4.99999
AlH ₂	1.78779	1.85225	4.84983	4.94506	3.06205	3.09281	4.99999	4.99999
Al ₂	1.35409	1.37642	5.21624	5.24844	3.86215	3.87203	5.99999	5.99999
PH	2.93432	2.98889	9.90272	9.98165	6.96840	6.99276	5.99999	5.99999
SiH ₂	2.49908	2.56394	7.42576	7.52084	4.92668	4.95690	5.99999	5.99999
SH	4.28212	4.34594	14.86480	14.96195	10.58268	10.61602	6.99999	6.99999
HSe	3.60975	3.66865	13.32892	13.41466	9.71917	9.74601	6.99999	6.99999
PH ₂	3.50459	3.57825	11.07451	11.17919	7.56992	7.60094	6.99999	6.99999
SiH ₃	3.12838	3.21874	8.58773	8.71139	5.45935	5.49265	6.99999	7.00000
HBr	4.79802	4.86591	18.47808	18.57517	13.68006	13.70926	7.99999	7.99999
MgS	4.03663	4.08783	14.90871	14.97037	10.87208	10.88254	8.00000	8.00000
NaBr	4.40312	4.45514	17.78349	17.85351	13.38037	13.39837	7.99999	7.99999
KCl	5.80442	5.86514	20.91611	21.00807	15.11169	15.14294	8.00001	8.00001
KBr	4.42002	4.47018	17.76799	17.83592	13.34797	13.36573	7.99999	7.99998
H ₂ Se	4.18273	4.26124	14.51438	14.62158	10.33165	10.36034	7.99999	7.99999
HI	3.65476	3.71595	15.57023	15.64787	11.91547	11.93191	7.99999	7.99999
SiH ₄	3.65832	3.76989	9.82333	9.97905	6.16500	6.20916	7.99999	8.00000
AlS	4.47030	4.52785	16.50709	16.57417	12.03680	12.04632	8.99999	8.99999
MgCl	5.96014	6.03442	21.70428	21.80874	15.74414	15.77432	8.99998	8.99999
P ₂	4.80329	4.86060	17.71797	17.77801	12.91468	12.91741	9.99999	10.00000
SiS	5.17566	5.23729	19.09644	19.16753	13.92078	13.93024	9.99999	9.99999
AlCl	6.33824	6.41277	23.24566	23.34650	16.90741	16.93374	9.99999	9.99999
PS	6.19564	6.27081	22.68040	22.77003	16.48476	16.49922	11.00000	11.00000
S ₂	7.58306	7.68138	27.62272	27.77409	20.03966	20.09271	12.00000	12.00000
Se ₂	6.21878	6.30169	24.55124	24.67301	18.33246	18.37132	11.99999	11.99999
PCl	8.05109	8.15428	29.34580	29.48093	21.29471	21.32664	12.00000	12.00000
BrCl	9.90905	10.03194	37.85211	38.01782	27.94306	27.98588	14.00000	14.00000
SiH ₃ Cl	8.82191	8.97475	29.32193	29.52706	20.50002	20.55231	14.00000	14.00000
SiCl ₂	12.71813	12.87162	46.37456	46.57075	33.65644	33.69913	17.99999	17.99999
S ₃	11.45897	11.59948	41.56900	41.72809	30.11003	30.12861	17.99999	17.99999
ClS ₂	13.29292	13.45889	48.23575	48.43954	34.94284	34.98065	19.00000	19.00000
P ₄	10.04128	10.15505	35.88401	35.95566	25.84274	25.80061	19.99999	19.99999
AlCl ₃	17.72370	17.94164	64.51025	64.79488	46.78655	46.85324	23.99999	23.99999
S ₂ Cl ₂	19.02565	19.26416	68.83640	69.12631	49.81075	49.86216	25.99999	25.99999
PCl ₃	19.50036	19.74348	70.61349	70.91249	51.11314	51.16902	26.00000	26.00000
SiHCl ₃	19.09265	19.34355	68.26422	68.57817	49.17157	49.23462	25.99999	25.99999
SiCl ₄	24.19691	24.50296	87.70251	88.07579	63.50560	63.57282	32.00000	32.00000
PCl ₅	30.92116	31.33096	111.74539	112.22809	80.82423	80.89713	40.00000	40.00000

from improper asymptotic *long-range* behavior. Consequently, whereas the ground-state total energies of atoms, molecules, solids can be predicted quite satisfactorily by using these functionals, the ionization energies obtained via the HOMO energies (usually off by 30-50% of the experimental values) as well as the excited states are described rather poorly. As mentioned in [23], our primary objective is to extend this scheme towards the dynamical studies of atoms and molecules under the influence of strong field such as a laser (through multi-photon ionization, high-order harmonic generation and other related phenomena) via TDDFT, that can potentially exploit the remarkable developments made in basis-set DFT through many pioneering works over the years. It is a necessary prerequisite that both the ionization potential and higher levels be described more accurately. Recently, the modified Leeuwen-Baerends (LB) potential [26, 27], $v_{xc\sigma}^{LB\alpha}(\alpha, \beta : \mathbf{r})$, containing two empirical parameters have been shown to be quite successful in dealing with the above dynamical situations of atoms, molecules (see, for example, [44], and the references therein) as well as for the static property calculations including TDDFT-based excited states of molecules. This is conveniently written as,

$$v_{xc\sigma}^{LB\alpha}(\alpha, \beta : \mathbf{r}) = \alpha v_{xc\sigma}^{LDA}(\mathbf{r}) + v_{xc\sigma}^{LDA}(\mathbf{r}) + \frac{\beta x_{\sigma}^2(\mathbf{r}) \rho_{\sigma}^{1/3}(\mathbf{r})}{1 + 3\beta x_{\sigma}(\mathbf{r}) \ln\{x_{\sigma}(\mathbf{r}) + [x_{\sigma}^2(\mathbf{r}) + 1]^{1/2}\}} \quad (8)$$

where σ signifies up,down spins and the last term containing gradient correction is reminiscent of the popular Becke exchange energy density functional [24], $x_{\sigma}(\mathbf{r}) = |\nabla\rho_{\sigma}(\mathbf{r})|[\rho_{\sigma}(\mathbf{r})]^{-4/3}$ is a dimensionless quantity, $\alpha = 1.19, \beta = 0.01$. This ensures the desired long-range property, i.e., $v_{xc\sigma}^{LB\alpha}(\mathbf{r}) \rightarrow -1/r, r \rightarrow \infty$. The HOMO energies, obtained from LBVWN (LB exchange and VWN correlation) combination are presented in column 4. It is abundantly clear that LBVWN results are significantly improved over either the LDA or BLYP cases. The LDA ionization energies are lower than BLYP values for all the molecules considered and LBVWN values are substantially lower than both these two. Evidently in our future work on TDDFT as mentioned above, this feature of LB potential will be highly exploited. Now columns 6, 7, 8 give the computed LDA, BLYP atomization energies and their experimental analogs. Here also both LDA and BLYP results show considerable deviation from the experimental values, which include zero-point vibrational corrections as well as relativistic effects. In many cases, LDA results are apparently better than their BLYP counterparts. However this observations should not be misconstrued to lead to the conclusion that former is a better candidate than the latter. We note that the

current work employs the Hay-Wadt-type *ab-initio* effective core potentials which are more suitable for the HF-type approaches. Among other factors, use of pseudopotentials and basis sets which are more appropriate for the DFT approaches, may alleviate some of the discrepancies encountered here and an undertaking along this direction may be initiated in future. Furthermore, large deviations in atomization energies have also been found in other recent DFT works involving all-electron calculations and more extended basis sets as well (see for example [45]). In any case, this is an evolving process and does not interfere with the main objective of the present work. Also note that there may be some cancellation of errors in the LDA case. Finally note that the extension of this approach to the “all-electron” atomic, molecular calculations as well as for very large systems would be relatively difficult compared to the present pseudopotential case in terms of the grid requirement, because of the presence of extra core electrons. Nevertheless reasonable *full* calculation of small to medium molecules are possible. This is suggested from some of our preliminary studies in this direction which I am currently engaged into and may be considered in some future communication.

IV. CONCLUDING REMARKS

Pseudopotential density functional calculations were performed for atoms and molecules within the LCGTF framework using CCG in conjunction with an accurate, efficient Fourier convolution technique to represent the classical Hartree potential in real grid. In essence, our previous work (I) on the LDA XC functionals has been extended to test its performance and validity in the case of gradient-corrected XC functionals which would be necessary for its further applications to realistic physical situations. For this purpose, the widely used BLYP XC functional was chosen. The calculated results of a variety of quantities such as energy components, eigenvalues, potential energy curves, ionization energies, atomization energies clearly reveal that, they are practically of the same quality as obtained from the available theoretical methods. Furthermore, companion LDA and BLYP calculations were performed for a large number of molecules (41) to illustrate its scope of applicability for a broad range of systems. Comparison with experiments has been made wherever possible. Additionally, for all the molecules studied, the LBVWN results show significant improvements in the HOMO energies. This has important relevance to our prospective future works on studying

TABLE VII: Negative HOMO energies, $-\epsilon_{\text{HOMO}}$ (in a.u.) and atomization energies (kcal/mol) for more molecules. LDA, LBVWN (LB+VWN), BLYP results are compared with experiment [43].

An asterisk indicates 298°K values. Otherwise, 0°K results are given. See text for details.

Molecule	$-\epsilon_{\text{HOMO}}$ (a.u.)				Atomization energy (kcal/mol)		
	LDA	BLYP	LBVWN	Expt. [43]	LDA	BLYP	Expt. [43]
Mg ₂	0.1563	0.1530	0.2316		4.04	0.22	0.9
MgH ₂	0.2248	0.2221	0.3471		113.75	109.09	
AlH	0.1741	0.1715	0.2836		72.65	68.31	70.3
SiH	0.1647	0.1597	0.2849	0.2900	74.47	69.59	70.4
AlH ₂	0.1655	0.1631	0.2755		127.69	118.90	114.7
Al ₂	0.1407	0.1400	0.2371	0.1984	22.92	21.42	37.0
PH	0.2214	0.2133	0.3519	0.3730	72.05	67.14	66.3
SiH ₂	0.2056	0.2027	0.3340	0.3278	155.85	143.93	144.1
SH	0.2229	0.2174	0.3736	0.3830	84.83	74.85	83.9
HSe	0.2117	0.2057	0.3534	0.3618	79.44	70.16	
PH ₂	0.2170	0.2111	0.3504	0.3610	152.77	139.92	149.2
SiH ₃	0.2017	0.1969	0.3278	0.2990	193.37	171.26	212.2
HBr	0.2688	0.2603	0.4147	0.4292	91.60	79.11	87.5*
MgS	0.1850	0.1766	0.2882		55.90	42.15	71.7
NaBr	0.1818	0.1729	0.3057	0.3050	87.47	78.94	86.8*
KCl	0.1481	0.1419	0.2805	0.3859	96.61	88.02	80.3*
KBr	0.1528	0.1449	0.2760	0.2903	87.39	79.35	69.8*
H ₂ Se	0.2152	0.2075	0.3524	0.3635	167.04	146.81	
HI	0.2518	0.2432	0.3824	0.3817	82.82	72.07	45.8*
SiH ₄	0.3188	0.3156	0.4624	0.4042	339.43	312.02	302.6
AlS	0.2342	0.2240	0.3497	0.3491	93.74	77.07	88.4
MgCl	0.1848	0.1804	0.2750	0.2753	78.76	68.47	76.5
P ₂	0.2590	0.2526	0.3877	0.3870	96.18	81.73	116.0
SiS	0.2565	0.2507	0.3828	0.3870	134.04	114.54	147.2
AlCl	0.2255	0.2204	0.3383	0.3454	115.69	100.65	119.2
PS	0.1695	0.1645	0.3054	0.3307	81.23	63.43	105.2
S ₂	0.2007	0.2023	0.3443	0.3438	56.75	52.47	100.8
Se ₂	0.1952	0.1951	0.3283	0.3160	58.40	54.78	
PCl	0.2093	0.2023	0.3490		65.12	49.37	71.7
BrCl	0.2623	0.2537	0.4133	0.4079	44.95	25.41	51.5
SiH ₃ Cl	0.2780	0.2704	0.4317	0.4267	337.97	300.07	321.7
SiCl ₂	0.2514	0.2448	0.3909	0.3804	190.40	155.11	202.7
S ₃	0.2392	0.2294	0.3805		116.84	72.14	
ClS ₂	0.2225	0.2161	0.3712		115.08	73.52	141.0
P ₄	0.2712	0.2575	0.3964	0.3432	200.77	142.99	285.9
AlCl ₃	0.3081	0.2976	0.4603	0.4414	278.02	232.88	303.4
S ₂ Cl ₂	0.2603	0.2499	0.4107	0.3550	151.27	90.54	192.2
PCl ₃	0.2747	0.2660	0.4266	0.3638	189.35	133.20	229.5
SiHCl ₃	0.3076	0.2971	0.4632		335.99	273.66	361.3
SiCl ₄	0.3194	0.3085	0.4758	0.4333	333.91	258.60	378.6
PCl ₅	0.2825	0.2722	0.4397	0.3748	246.22	145.33	303.2

real-time dynamics of atoms and/or molecules in a strong laser field. Incorporation of other pseudopotentials more suited to DFT as well as more extended and elaborate basis sets would be among some of the important issues which may be considered in recent future. More accurate XC functionals could also be employed depending upon the physical system concerned and the nature of the problem dealt with. Applications to weakly bonded systems, clusters and of course, to larger systems would further consolidate its success. Finally although one could think of some inherent errors associated with the incompleteness of the grid, this study confirms that with a judicious choice of the grid coupled with a correct treatment of the Coulomb potential, these can be reduced to tolerable minima. Thus very satisfactory results could be obtained.

Acknowledgments

The project was initiated at Prof. D. Neuhauser's laboratory at the Univ. of California, Los Angeles, where the core of the program was written. It was further extended at Prof. S. I. Chu's laboratory at the University of Kansas. I thank them for stimulating discussions and providing the computational facilities. Numerous useful discussions with Dr. E.I. Proynov is gratefully acknowledged. Warm hospitality offered by UCLA and the Univ. of Kansas is greatly appreciated. An anonymous referee is thanked for valuable constructive comments.

-
- [1] S. R. White, J. W. Wilkins and M. P. Teter, Phys. Rev. B **39**, 5819 (1989).
 - [2] J. R. Chelikowsky, N. Troullier, K. Wu and Y. Saad, Phys. Rev. B **50**, 11355 (1994).
 - [3] E. L. Briggs, D. J. Sullivan and J. Bernholc, Phys. Rev. B **52**, R5471 (1995).
 - [4] F. Gygi and G. Galli, Phys. Rev B **52**, R2229 (1995).
 - [5] T. L. Beck, Rev. Mod. Phys. **72**, 1041 (2000).
 - [6] T. Helgaker, P. Jorgensen and J. Olsen, *Molecular-Electronic Structure Theory* (John-Wiley & Sons Ltd., 2000).
 - [7] M. C. Payne, M. P. Teter, D. C. Allan, T. A. Arias and J. D. Joannopoulos, Rev. Mod. Phys. **64**, 1045 (1992).

- [8] M. Krack and M. Parinello, *Phys. Chem. Chem. Phys.* **2**, 2105 (2000).
- [9] Y. C. Zheng and J. Almlöf, *Chem. Phys. Lett.* **214**, 397 (1993).
- [10] A. D. Becke, *J. Chem. Phys.* **88**, 2547 (1988).
- [11] O. Treutler and R. Ahlrichs, *J. Chem. Phys.* **102**, 346 (1995).
- [12] M. M. Mura and P. J. Knowles, *J. Chem. Phys.* **104**, 9848 (1996).
- [13] C. W. Murray, N. C. Handy and G. J. Laming, *Mol. Phys.* **78**, 997 (1993).
- [14] P. M. W. Gill, B. G. Johnson and J. A. Pople, *Chem. Phys. Lett.* **209**, 506 (1993).
- [15] R. Lindh, P. -A. Malmqvist and L. Gagliardi, *Theor. Chem. Acc.* **106**, 178 (2001).
- [16] V. I. Lebedev and Zh. Vychisl, *Mat. Mat. Fiz.* **15**, 48 (1975).
- [17] V. I. Lebedev and Zh. Vychisl, *Mat. Mat. Fiz.* **16**, 293 (1976).
- [18] V. I. Lebedev and A. L. Skorokhodov, *Russ. Acad. Sci. Dokl. Math.* **45**, 587 (1992).
- [19] P. M. Boerrigter, G. Te. Velde and E. J. Baerends, *Int. J. Quant. Chem.* **33**, 87 (1988).
- [20] M. R. Pederson and K. A. Jackson, *Phys. Rev. B* **41**, 7453 (1990).
- [21] X. Chen, J.-M. Langlois and W. A. Goddard III, *Phys. Rev. B* **52**, 2348 (1995).
- [22] J. Kong, S. T. Brown and L. Füsti-Molnár, *J. Chem. Phys.* **124**, 094109 (2006).
- [23] A. K. Roy, *Int. J. Quant. Chem.* **108**, 837 (2008).
- [24] A. D. Becke, *Phys. Rev. A* **38**, 3098 (1988).
- [25] C. Lee, W. Yang and R. G. Parr, *Phys. Rev. B* **37**, 785 (1988).
- [26] R. van Leeuwen and E. J. Baerends, *Phys. Rev. A* **49**, 2421 (1994).
- [27] P. R. T. Schipper, O. V. Gritsenko, S. J. A. van Gisbergen and E. J. Baerends, *J. Chem. Phys.* **112**, 1344 (2000).
- [28] S. Obara and A. Saika, *J. Chem. Phys.* **84**, 3963 (1986).
- [29] L. E. McMurchie and E. R. Davidson, *J. Comput. Phys.* **26**, 218 (1978).
- [30] M. W. Schmidt, K. K. Baldrige, J. A. Boatz, S. T. Elbert, M. S. Gordon, J. H. Hensen, S. Koseki, N. Matsunaga, K. A. Nguyen, S. J. Su, T. L. Windus, M. Dupuis and J. A. Montgomery, *J. Comput. Chem.* **14**, 1347 (1993).
- [31] G. C. Martyna and M. E. Tuckerman, *J. Chem. Phys.* **110**, 2810 (1999).
- [32] P. Minary, M. E. Tuckerman, K. A. Pihakari and G. J. Martyna, *J. Chem. Phys.* **116**, 5351 (2002).
- [33] B. Miehl, A. Savin, H. Stoll and H. Preuss, *Chem. Phys. Lett.* **157**, 200 (1989).
- [34] S. H. Vosko, L. Wilk and M. Nusair, *Can. J. Phys.* **58**, 1200 (1980).

- [35] J. A. Pople, P. M. W. Gill and B. G. Johnson, *Chem. Phys. Lett.* **199**, 557 (1992).
- [36] *Density Functional Repository*, Quantum Chemistry Group, CCLRC Daresbury Laboratory, Daresbury, Cheshire, WA4 4AD, UK.
- [37] J. Andzelm and E. J. Wimmer, *J. Chem. Phys.* **96**, 1280 (1992).
- [38] E. J. Baerends, D. E. Ellis and P. Ros, *Chem. Phys.* **2**, 41 (1973).
- [39] H. Sambe and R. H. Felton, *J. Chem. Phys.* **62**, 1122 (1975).
- [40] B. I. Dunlap, J. W. D. Connolly and J. R. Savin, *J. Chem. Phys.* **71**, 4993 (1979).
- [41] E. Anderson, Z. Bai, C. Bischof, S. Blackford, J. Demmel, J. Dongarra, J. Du Croz, A. Greenbaum, S. Hammarling, A. McKenney, D. Sorensen, *LAPACK Users' Guide*. 3rd Ed. (SIAM, Philadelphia, 1999).
- [42] R. D. Johnson III (Ed.), *NIST Computational Chemistry Comparison and Benchmark Database, NIST standard Reference Database*. Number 101. Release 14, Sept. 2006. (<http://srdata.nist.gov/cccbdb>).
- [43] H. Y. Afeefy, J. E. Liebman and S. E. Stein, "Neutral Thermochemical Data" in *NIST Chemistry WebBook, NIST Standard Reference Database Number 69*, Eds. P. J. Linstrom and W. G. Mallard, June 2005, National Institute of Standards and Technology, Gaithersburg MD, 20899. (<http://webbook.nist.gov>).
- [44] S. I. Chu, *J. Chem. Phys.* **123**, 062207 (2005).
- [45] M. Cafiero, *Chem. Phys. Lett.* **418**, 126 (2006).